IEEE Access
Multidisciplinary | Rapid Review | Open Access Journal

Received January 22, 2022, accepted February 1, 2022, date of publication February 9, 2022, date of current version February 16, 2022.

Digital Object Identifier 10.1109/ACCESS.2022.3150316

Step-Up DC-DC Switching Converter With Single Switch and Multi-Outputs Based on Luo Topology

FERESHTEH GHASEMI, MOHAMMAD ROUHOLLAH YAZDANI, (Member, IEEE), AND MAJID DELSHAD

Department of Electrical and Computer Engineering, Islamic Azad University, Isfahan (Khorasgan) Branch, Esfahan 81551-39998, Iran

Corresponding author: Mohammad Rouhollah Yazdani (m.yazdani@khuisf.ac.ir)

ABSTRACT In this paper, a step-up DC-DC multi-output converter is introduced by integrating a super-lift Luo converter, flyback topology, and coupled inductor concept. The proposed multi-output converter has positive output super-lift structure while simultaneously generating step-up voltages in its outputs. The proposed step-up converter has two non-isolated and one isolated output with a simple structure using one switch and one magnetic core. There is no voltage spike by the leakage inductance of the coupled inductor across the switch in the proposed converter. Therefore, the switch has low-stress voltage. The energy in the leakage inductor is recycled leading to higher efficiency in comparison to similar converters with the coupled inductor. The operating principles and the characteristics of the proposed converter are analyzed and discussed. The experimental results of 110W prototype verify the theoretical analysis and the benefits of the proposed converter in comparison to similar multi-output converters. The conducted electromagnetic interference evaluation of the proposed converter is presented and it is reduced using a common-mode choke.

INDEX TERMS Conducted EMI, coupled inductor, Luo converter, multi-outputs, step-up DC-DC conversion.

I. INTRODUCTION

Over the last few decades, power DC-DC converters have been the subject of great concern due to their wide increase of utilization in different applications [1]. Step-up DC-DC converters are widely used in numerous power conversion applications and converting lower power DC levels to higher levels. The energy can be stored either in magnetic components as single/coupled inductor or in electric field components as capacitors by active or passive power switching elements. Step-up DC-DC converters are used in portable device applications, aerospace, satellite application, hybrid electric vehicles, and photovoltaic systems [2]–[5].

Step-up DC-DC converters can be divided into isolated and non-isolated converters. Boost converter as a regular non-isolated converter provides high-voltage gain with working at a higher duty ratio. Different topologies of step-up DC-DC non-isolated converters are proposed to improve voltage gain and efficiency. In some applications, isolated converters are chosen to meet the safety standards, provide galvanic isolation, and enhance noise immunity. Flyback converter as a conventional isolated step-up converter is used in low power applications together with multiple outputs due to the low number of elements, modest construction, and low cost [6]. In [7], an integrated topology with flyback converter in a single-stage structure is presented to suggest flexible step-up DC-DC converters. Coupled inductor is often selected due to its reduced component count, better integration, and lower inductance requirement compared to uncoupled inductor [8], [9]. However, coupled-inductors can provide a high step-up ratio with a low operating duty cycle using desire turn ratio, and consequently increasing power converter efficiency considerably [10], [11]. Flyback converter can be integrated with other topology using coupled inductor; high-voltage gain of these converters can be achieved by adjusting turns ratio of coupled inductor [12], [13].

The power converter of a single input source and multiple outputs with various voltage is known as a single-input multiple-output converter (SIMO) [14]. The single-input multi-output converter is becoming the cost-effective choice instead of hiring multi single-input single-output converters [2]. SIMO can be isolated type or non-isolated; isolated-type has multiple winding transformers to employ for multiple loads [15]. Generally, multi-output converters can be widely used in renewable energy [16]–[18],

The associate editor coordinating the review of this manuscript and approving it for publication was Zhilei Yao.

electric vehicles [19], [20], DC Nano-grids [21], small satellites [22], power charger-supply applications [23], and LED driver [24]. In [24], a multi-output converter for the LED driver is proposed using two transformers and three switches. However, there are voltage spikes across the switches yielding electromagnetic emissions and higher switch stress. A switched boost dual output converter is designed for solar power applications but three switches are needed for dual outputs [15]. A single-input three-output converter with low voltage stresses on semiconductors, for low power applications of an electric vehicle or in Green houses is presented in [19]. However, many components have been made a complex circuit along with decreasing efficiency in the mentioned converter.

Step-up multi-output converters can employ boost, SEPIC, Cuk, and Luo topologies. Luo converters are a series of DC-DC step-up developed-type converters with a simple circuit structure, high efficiency, and low current and voltage ripple. Luo converters with the voltage-lift (VL) technique have a higher voltage gain than the regular boost converter. Super lift Luo converter significantly increases voltage transfer gain stage by stage [25], [26]. Positive output super lift converters are divided into some series based on voltage increment, number of the inductors, and capacitors. Each circuit of the main series has one switch, n inductors, 2n capacitors, and (3n-1) diodes for the n^{th} stage circuit [27]. The voltage-lift and coupled inductor techniques are good combinations to meet high step-up voltage gain for a converter [28]. Interleaved Luo converter deals with reducing circuit component count in addition to power quality enhancement. Using Luo converter along with conventional step-up converters would improve both circuit limitations; lowering switch stresses as well as expanding the area of operating in continuous conduction mode (CCM) [29], [30].

One way to obtain a proper step-up ratio in converters is to use a positive output super-lift Luo DC-DC converter (POSLLC). POSLLC is more powerful than boost, CUK, and SEPIC converters, It has higher efficiency, good power density, higher voltage transfer gain, and large voltage amplification [31]. Generally, the positive super-lift Luo converter shown in Fig. 1 operates in continuous conduction mode (CCM), with two different work states during one switching period.

In this paper, a single-switch step-up converter is proposed with multi-outputs based on positive output super-lift Luo topology to provide two non-isolated outputs and one isolated output. Multiple outputs of the proposed converter are achieved by integrating a flyback converter, super lift Luo converter, and coupled inductor with a single switch. Since all inductors are on one core, the size of the converter is reduced in comparison to multi-output converters with two transformers. Despite regular coupled inductor converters, the energy of the leakage inductances is recycled to eliminate voltage spikes across the switch leading to higher efficiency and lower electromagnetic emissions. The proposed converter can be utilized for supplying midlevel voltage dc loads in some multi-output applications like electric vehicles or renewable energy systems.

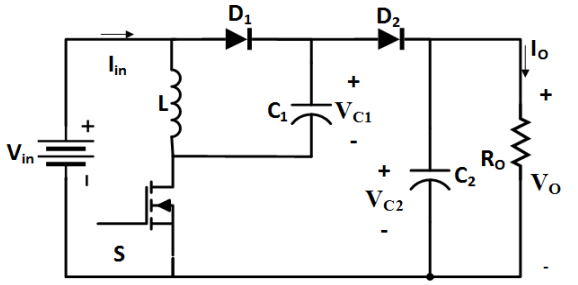

FIGURE 1. Positive output super-lift Luo DC-DC converter [27].

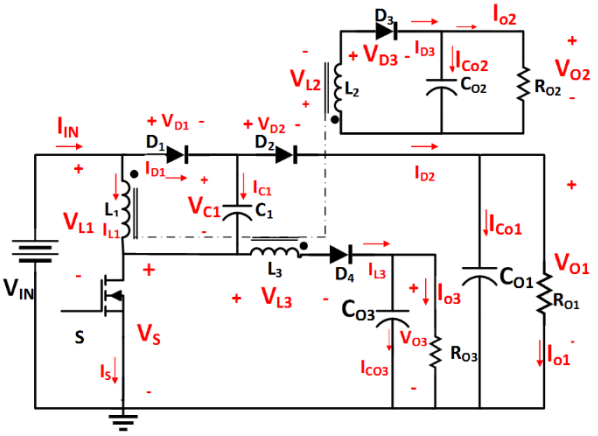

FIGURE 2. Multi-output single–switch proposed converter.

This paper is organized as follows. Section II presents the theoretical analysis and operation intervals of the proposed converter. In section III, the design considerations and dynamics of the proposed converter are discussed. Section IV presents the results to show the experimental waveforms with a comparison among step-up converters. The conducted electromagnetic interference (EMI) of the proposed converter is measured in section V. Finally, concluding remarks are offered in section VI.

II. OPERATING PRINCIPLES

The proposed converter is shown in Fig. 2. The positive output super-lift Luo DC-DC converter (POSLLC) in Fig. 1, is integrated with the flyback topology and coupled inductor. It poses three outputs with one single switch and one coupled inductor. As shown in Fig. 2, the proposed converter involves input source V_{in}, three coupled inductor L_1, L_2, and L_3 on one core, capacitors C_1, C_{O1}, C_{O2}, and C_{O3} and diodes D_1, D_2, D_3, and D_4 with a switch, S. The regular pulse-width-modulation (PWM) can be used for the converter control scheme.

To analyze the proposed converter, the following conditions are supposed:

1) The converter operates under CCM.
2) Forward voltage drop of the diodes, the equivalent series resistance of the coupled inductor and output capacitors are neglected.

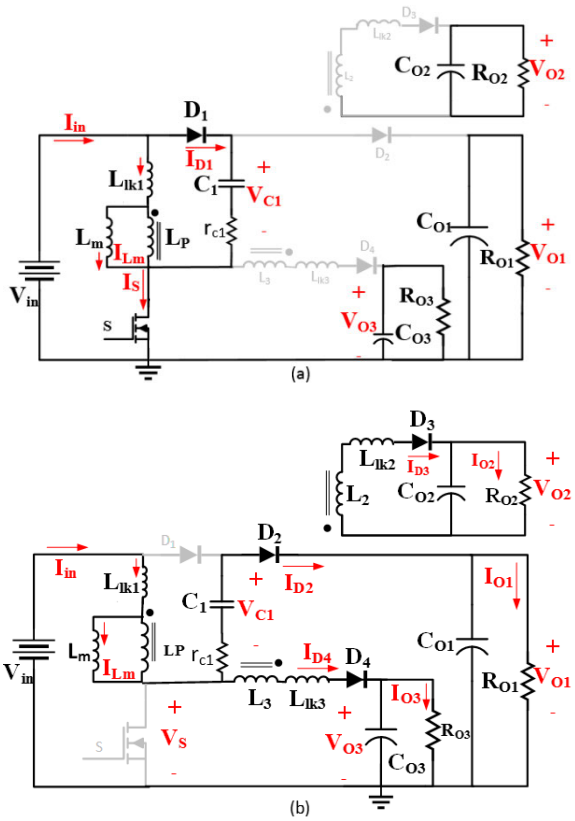

FIGURE 3. Equivalent circuit for each of the operating modes. (a) First mode, the switch is on. (b) Second mode, the switch is off.

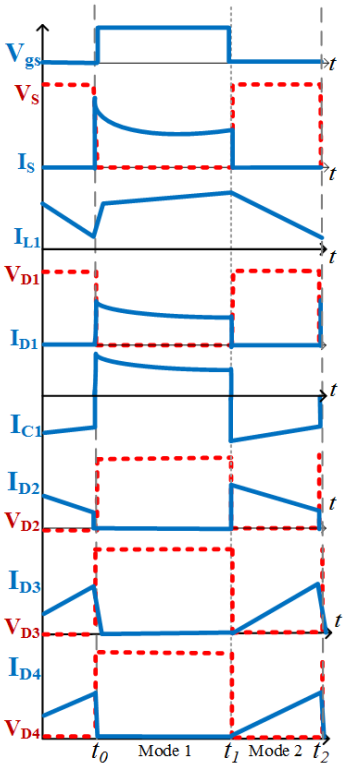

FIGURE 4. Theoretical waveforms of the proposed converter.

3) Equivalent series resistance (ESR) of C_1, is modeled by r_{c1}.
4) Capacitors Co_1, Co_2, and Co_3 are assumed constant.
5) A magnetizing inductor L_m, leakage inductances L_{lk1}, L_{lk2}, and L_{lk3} are used to model coupled inductor and L_m is large enough.
6) The primary coupled inductor L_1 has n_1 turns; n_2 and n_3 are the number of turns for L_2 and L_3 respectively. Coupled inductors turn ratios are:

$$N_A = \frac{n_1}{n_3}, \quad N_B = \frac{n_2}{n_1} \tag{1}$$

The proposed converter has three basic modes, which are illustrated in Fig. 3. The typical key waveforms at the steady-state condition are also shown in Fig. 4.

The operating modes are described as follows:

Mode I, $[t_0, t_1]$; *Fig. 3a:* this mode starts by turning on the switch at t_0. The current flows through L_{lk1},L_m, and C_1. In this mode, the voltage across D_1 reaches zero and it turns on. Diode D_2, D_3, and D_4 is reverse biased and the magnetizing inductor L_m is charged.

The important equations of this mode are as follows:

$$I_{lk1}(t) = I_{Lm}(t_0) + \frac{V_{in} - V_{Lm}}{L_{lk1}}(t - t_0) \tag{2}$$

$$I_{Lm}(t) = I_{Lm}(t_0) + \frac{V_{in} - V_{lk1}}{L_m}(t - t_0) \tag{3}$$

$$I_{C1}(t) = \frac{V_{in} - V_{C1}(t_0)}{r_{C1}} e^{-(t-t_0)/\tau} \tag{4}$$

where

$$\tau = r_{C1} C_1 \tag{5}$$

The switch current $I_s(t)$ is:

$$I_S(t) = I_{C1}(t) + I_{lk1}(t) \tag{6}$$

The C_1 charging current appear exponentially in this mode. The initial value of the charging current depends on the initial voltage across C_1, the ESR of C_1, and the resistance of the switch. r_{C1} as a major parasitic component serves to limit the peak amplitude of the charging current. At the end of this mode, the voltage across capacitor C_1 reaches about V_{in}, and diode D_1 is turned off. The energy is stored in the magnetizing inductance L_m in this interval. The loads R_{O1}, R_{O2}, and R_{O3} are supplied through the discharging output capacitors C_{O1}, C_{O2}, and C_{O3} respectively.

Mode II, $[t_1, t_2]$; *Fig. 3b:* The switch is turned off at t_2. Currents of leakage and magnetizing inductance L_{lk1} and L_m decrease linearly. Diodes D_2, D_3, and D_4 conducts due to their forward bias and the power is transferred to outputs via coupled inductors L_2 and L_3. Since D_2 is on, D_1 remains off at this mode. The stored energy of C_1 starts to transfer the output branch C_{O1} and R_{O1}. The flyback section consists of D_3, L_2, C_{O2}, and R_{O2}, where the energy is delivered to the load by L_2 and leakage inductor L_{lk2}. C_{O3} has become positive and starts to be charged via L_3 and leakage inductor L_{lk3}.

Stored energy in the leakage inductance L_{lk1} absorbs by capacitor C_1 so the voltage spikes on the switch are escaped which is an important feature of the proposed converter. The currents of the leakage and magnetizing inductor are expressed by the following equations:

$$I_{lk1}(t) = I_{Lm}(t_1) + \frac{V_{lk1}}{L_{lk1}}(t - t_1) \tag{7}$$

$$I_{Lm}(t) = I_{Lm}(t_1) + \frac{2V_{in} - V_{lk1} - V_{o1}}{L_m}(t - t_1) \tag{8}$$

$$I_{C1}(t) = I_{Lm}(t) + I_{L3}(t) \tag{9}$$

where:

$$I_{Lm} = N_B I_{L2} - \frac{I_{L3}}{N_A} \tag{10}$$

III. ANALYSIS OF THE PROPOSED CONVERTER

In order to design the converter, selecting the appropriate values of L_m, N_A, N_B, C_o, and the value of duty cycle (d) are vital. Design consideration is classified from conversion gains to losses as well as dynamics.

A. CONVERSION GAINS

The voltage conversion ratio is calculated by volt-second balance of the inductors:

$$\frac{V_{in}}{L_m}dT + \frac{2V_{in} - V_{o1}}{L_m}(1-d)T = 0 \tag{11}$$

$$\frac{V_{in}}{L_m}dT - \frac{V_{o2}}{L_m N_B}(1-d)T = 0 \tag{12}$$

$$\frac{V_{in}}{L_m}dT + \frac{V_{in} - V_{o3}}{L_m(1 + \frac{1}{N_A})}(1-d)T = 0 \tag{13}$$

Consequently, voltage gains are presented in (14), (15), and (16):

$$G_1 = \frac{V_{o1}}{V_{in}} = \frac{2-d}{1-d} \tag{14}$$

$$G_2 = \frac{V_{o2}}{V_{in}} = \frac{dN_B}{1-d} \tag{15}$$

$$G_3 = \frac{V_{o3}}{V_{in}} = \frac{1 + \frac{d}{N_A}}{1-d} \tag{16}$$

For a better comparison, Fig. 5 illustrates a plot of three voltage gains versus duty cycle of the proposed converter for the turns-ratio N_A and N_B equal to two. Fig. 6 shows plot of the voltage gain of flyback part in the proposed converter versus duty cycle considering different turns ratios. This output provides an isolated one and can be adjusted by turns ratio N_B. In addition, voltage gain and duty cycle curves under various turns ratios are plotted in Fig. 7 for output 3.

B. DESIGN OF COUPLED INDUCTOR

Turn ratios of the coupled inductor can be determined according to desired gains using (14), (15), and (16). In the proposed converter, transferring energy to the output stage rests on the magnetizing inductance. To determine the current and value of the magnetizing inductance, the following procedure is used.

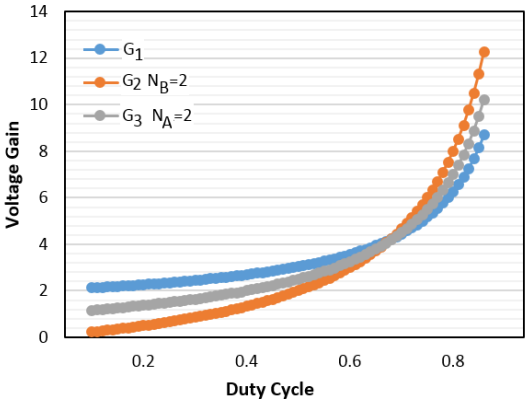

FIGURE 5. Voltage gains versus duty cycle plot.

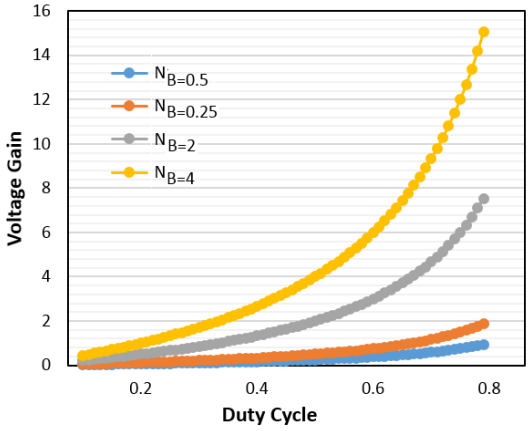

FIGURE 6. Plot of G2 versus duty ratio for different turn ratio.

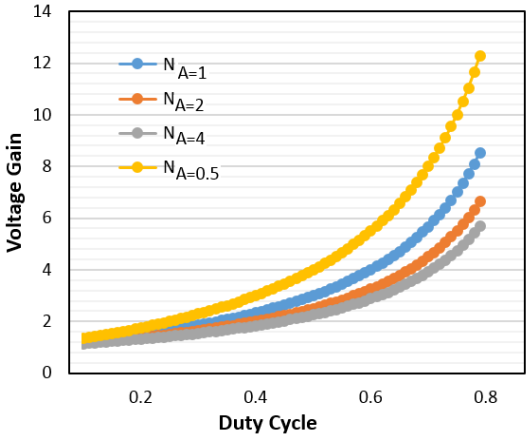

FIGURE 7. Plot of G3 versus duty ratio for different turn ratio.

The voltage across L_m is:

$$V_{Lm} = L_m \frac{\Delta i_{Lm}}{\Delta t} \tag{17}$$

V_{in} is applied across L_m, so:

$$L_m = V_{in} \frac{d}{f \Delta i_{Lm}} \tag{18}$$

In order to guarantee the operation of in CCM, the average current through the magnetic inductance, L_m, should be more than half of the inductor current ripple. The variation ratio of current i_{Lm} through L_m is:

$$\xi = \frac{\Delta i_{Lm}}{2I_{Lm}} < 1 \tag{19}$$

In the proposed converter, ξ is designed much lower than unity, to confirm that it normally works in the continuous mode. Moreover, the average current of the magnetizing inductance L_m is achieved as given in (20):

$$I_{Lm} = I_{in} - I_{O1}\frac{1}{d} \tag{20}$$

The stability of the magnetizing current is also considered in the design of the magnetizing inductance. Therefore, by using (18) and (20), the magnetizing inductance for the presented converter is obtained as follows:

$$L_m \geq d^2(1-d)/2f(2-d)\left[\frac{dI_{in}}{V_{O1}} - \frac{1}{R_{O1}}\right] \tag{21}$$

For known turn ratio considering desired gains, the inductors ratios are determined with approximation as below:

$$L_1 = \left(\frac{1}{N_B}\right)^2 L_2 \tag{22}$$

$$L_1 = (N_A)^2 L_3 \tag{23}$$

C. OUTPUT CAPACITORS

Based on two main modes, the appropriate value of C_1 is determined considering discharging time interval of the capacitor, that is, (1−d)T. The equality in (24) should be satisfied with a peak-to-peak voltage ripple of C_1:

$$C_1 = \frac{I_{O1}d}{f_s \Delta V_{C1}} \tag{24}$$

In view of the effect of the capacitor voltage drop, the output voltage ripples should be attended. Therefore, Ro_1, and the C_1 value should not be too small moreover, f_s should not be too low. C_{O1}, C_{O2}, and C_{O3} can be found using the amp-sec balance principle:

$$C_{O1,O2,O3} = \frac{(1-d)}{f_s R_{O1,O2,O3}(\Delta V_{O1,O2,O3}/V_{O1,O2,O3})} \tag{25}$$

D. COMPONENT VOLTAGE AND CURRENT STRESSES

In the first mode, the switch is on, so the following equations can be written for capacitors' currents based on Fig. 3:

$$I_{C1-on} = I_{D1} = -I_{Lm-on} + I_{in} \tag{26}$$

$$I_{CO1,CO2,CO3-on} = I_{O1,O2,O3-on} \tag{27}$$

At mode II, the switch is off and the capacitors' currents can be expressed as follows:

$$I_{C1-off} = I_{D2} = -I_{D4} + I_{in} \tag{28}$$

$$I_{CO1-off} = I_{D2} - I_{O1-Off} \tag{29}$$

$$I_{CO2-off} = I_{D3} - I_{O2-Off} \tag{30}$$

$$I_{CO3-off} = I_{D4} - I_{O3-Off} \tag{31}$$

The amp-sec balance to all capacitors, the equations can be derived as:

$$I_{CX-on}d = I_{CX-off}(1-d)x = 1, 2, o_1, o_2 \tag{32}$$

Considering that the load is resistive:

$$I_{Lm-on} = I_{Lm-off} = I_{Lm} \tag{33}$$

$$I_{out-on} = I_{out-off} = I_{out} \tag{34}$$

By substituting (26)-(31), into (32) the current of capacitors in mode I can be deduced as follows:

$$I_{C1-on} = I_{D1} = I_{O1}\frac{1}{d} \tag{35}$$

$$I_{CO1,CO2,CO3-on} = I_{O1,O2,O3} \tag{36}$$

In addition, the currents of capacitors in mode II are:

$$I_{C1-off} = I_{D2} = I_{O1}\frac{1}{1-d} \tag{37}$$

$$I_{CO1,CO2,CO3-off} = I_{O1,O2,O3}\frac{d}{1-d} \tag{38}$$

Considering the above equations, the mean stress of semiconductors' currents during two modes can be obtained. The current and voltage on diodes and the switch are listed in Table 1.

TABLE 1. Voltage and current stresses.

Item	Stress Values
$\mathbf{V_s}$	$\frac{V_{in}}{1-d}$
$\mathbf{I_s}$	I_{in}
$\mathbf{V_{D1}, V_{D2}}$	$V_{O1} - V_{in}$
$\mathbf{I_{D1}}$	$I_{O1}\frac{1}{d}$
$\mathbf{I_{D2}}$	$\frac{I_{O1}}{1-d}$
$\mathbf{I_{D3}}$	$I_{O2}\frac{1}{1-d}$
$\mathbf{I_{D4}}$	$I_{O3}\frac{1}{1-d}$
$\mathbf{V_{D3}}$	$V_{O2} + N_B V_{in}$
$\mathbf{V_{D4}}$	$V_{O3} + (V_{in}/N_A)$

It can be concluded that the switch voltage stress of the proposed converter has no relation with the turn-ratio of the coupled inductor and can be related to the duty cycle and input voltage; however, in the single switch multi-output converters there are some design limitations due to a unique duty cycle and turn ratios.

TABLE 2. RMS current stresses.

Item	RMS Value
I_{s-rms}	$I_{in}\sqrt{d}$
I_{D1-rms}	$I_{O1}\frac{1}{\sqrt{d}}$
I_{D2-rms}	$\frac{I_{o1}}{1-d}\sqrt{1-d}$
I_{D3-rms}	$\frac{I_{o2}}{1-d}\sqrt{1-d}$
I_{D4-rms}	$\frac{I_{o3}}{1-d}\sqrt{1-d}$

E. RMS CURRENTS AND POWER LOSSES

The efficiency value of the proposed converter is achieved considering losses. Power losses are estimated supposing the inductor currents are ripple-free. RMS currents are shown in Table. 2.

In order to calculate the efficiency of the proposed converter, main losses must be included in power loss analysis.

Therefore, power losses of the proposed converter can be considered into four sets: (i) switch loss, (ii) diodes loss, (iii) (ESR) (r_c) loss, and (iv) magnetic components loss. In this part, it should be mentioned that capacitors ESRs, are supposed to be equal.

The power losses of power switch are equal to the summation of switching and conduction losses. Considering r_{on} as on-resistance of the switch, conduction losses is:

$$P_{s-con} = r_{on} i^2_{s-rms} = r_{on} I^2_{in} d \tag{39}$$

Considering switch output capacitance C_s as a linear element, switching loss is calculated by:

$$P_{sw} = f_s C_s V^2_{S-stress} = \frac{f_s C_s}{2} (V_{O1} - V_{in})^2 \tag{40}$$

Total power loss in the switch without drive power loss is:

$$P_{s-TLoss} = P_{s-con} + P_{sw} \tag{41}$$

The total power losses in the diodes are the summation of power losses in forward resistance r_f and threshold voltages V_F:

$$P_{D-Tloss} = P_{r-on} + P_{VF} = r_f I^2_{D-rms} + V_f I_{D-ave} \tag{42}$$

$$P_{D1-Tloss} = r_{F-D1} \frac{I_{O1}}{d}^2 + V_{F-D1} I_{O1} = A_1 \tag{43}$$

$$P_{D2-Tloss} = r_{F-D2} \frac{I_{O1}}{1-d}^2 + V_{F-D2} I_{O1} = A_2 \tag{44}$$

$$P_{D3-Tloss} = r_{F-D3} \frac{I_{O2}}{1-d}^2 + V_{F-D3} I_{O2} = A_3 \tag{45}$$

$$P_{D4-Tloss} = r_{F-D4} \frac{I_{O3}}{1-d}^2 + V_{F-D4} I_{O3} = A_4 \tag{46}$$

$$P_{D-Tloss} = A_1 + A_2 + A_3 + A_4 \tag{47}$$

The losses of coupled inductor are divided into core and copper losses. Core losses considerably contribute to the temperature rise of coupled inductor, so it is not neglected in the power loss calculations; Winding coil losses or copper losses due to skin effect, proximity effect, the effect of eddy currents in the windings, and edge effects may be significant. Although, for simplicity, these additional winding losses are ignored and just RMS value of the coupled inductor current is estimated for copper losses.

$$P_{L-Loss} = k(f\ (\Delta B) + r_L I^2_{L-rms} \tag{48}$$

The ESR of the inductor L also causes some power loss. Since the current ripples across the inductors are not considered, the RMS value of the coupled inductor current is considered equal with its average value so the copper losses in windings are expressed in (49), (50), and (51):

$$P_{L1-Lcopper} = r_{L1} \left(I_{in} - \frac{V_{O1}}{dR_{O1}} \right)^2 \tag{49}$$

$$P_{L2-Lcopper} = r_{L2} \left(I_{O2} \frac{1}{1-d} \right)^2 \tag{50}$$

$$P_{L3-Lcopper} = r_{L3} \left(I_{O3} \frac{1}{1-d} \right)^2 \tag{51}$$

$$P_{L-Tloss} = P_{L1-Lcopper} + P_{L2-Lcopper} + P_{L3-Lcopper} \tag{52}$$

The capacitors' lead inductance is ignored and it is not considered as a part of the circuit. In addition, the power losses in capacitor ESRs are given by:

$$P_{C-Loss} = r_C I^2_{C-rms} = r_C \left[\begin{array}{l} I_{O1} \left(\frac{1}{\sqrt{d}} + \frac{1}{\sqrt{1-d}} \right) + \\ (I_{O1} + I_{O3} + I_{O2}) \left(\sqrt{d} + \frac{d}{\sqrt{1-d}} \right) \end{array} \right]^2 \tag{53}$$

Eventually, the overall power loss is estimated by the following equation:

$$P_{Loss} = P_{S-Loss} + P_{D-loss} + P_{L-Loss} + P_{C-Loss} \tag{54}$$

F. DYNAMIC PERFORMANCE

To obtain transfer functions, the average state-space method is utilized. The state equations and output variables are given in state-space form as follows:

$$\begin{cases} \left[\hat{x}_i(t)\right] = [A]\left[\hat{x}_i(t)\right] + [B]\left[\hat{u}_i(t)\right] \\ \left[\hat{y}_i(t)\right] = [C]\left[\hat{x}_i(t)\right] + [D]\left[\hat{u}_i(t)\right] \end{cases} \tag{55}$$

The state and input variable vectors are specified as:

$$\left[\hat{x}\right] = \left[\hat{i}_{L1}, \hat{i}_{L2}, \hat{i}_{L3}, \hat{v}_{C1}, \hat{v}_{CO3}, \hat{v}_{CO1}, \hat{v}_{CO2}\right] \tag{56}$$

$$\left[\hat{u}\right] = \left[\hat{v}_{in}\right] \tag{57}$$

$$\left[\hat{y}\right] = \left[\hat{v}_{O1}, \hat{v}_{O2}, \hat{v}_{O3}\right] \tag{58}$$

TABLE 3. Prototype specification.

Parameter	Value
Input voltage	12V
Output Power	110W
Switching frequency	115kHz
N_A, N_B	2
Duty cycle (d)	0.66
L_m	197 µH
L_{lk1}, L_{lk2}, L_{lk3}	2.6µH, 4.8µH, 1.8µH
C_1	47µf
C_{O1}, C_{O2}, C_{O3}	100µf
V_{O1}, V_{O2}, V_{O3}	48V, 36V, 24V

The matrixes related to (55) are given as follows:

$$A = \begin{bmatrix} 0 & 0 & 0 & \frac{-1}{L_1} & 0 & \frac{-(1-d)}{L_1} & 0 \\ 0 & 0 & 0 & 0 & 0 & 0 & \frac{-(1-d)}{L_2} \\ 0 & 0 & 0 & \frac{-(1-d)}{L_3} & \frac{-(1-d)}{L_3} & \frac{1-d}{L_3} & 0 \\ \frac{1-d}{C_1} & 0 & \frac{1-d}{C_1} & 0 & 0 & 0 & 0 \\ 0 & 0 & \frac{1-d}{C_{O3}} & 0 & \frac{-1}{C_{O3}R_{O3}} & 0 & 0 \\ \frac{1-d}{C_{O1}} & 0 & \frac{-(1-d)}{C_{O1}} & 0 & 0 & \frac{-1}{C_{O1}R_{O1}} & 0 \\ 0 & \frac{1-d}{C_{O2}} & 0 & 0 & 0 & 0 & \frac{-1}{C_{O2}R_{O2}} \end{bmatrix} \tag{59}$$

The dynamic performance can be analyzed with small-signal frequency response. Bode plots responses are presented in Fig. 8.

$$B = \begin{bmatrix} \frac{1-d}{L_1} \\ 0 \\ 0 \\ 0 \\ 0 \\ 0 \\ 0 \end{bmatrix}; \quad C = \begin{bmatrix} 0\,0\,0\,0\,0\,1\,0 \\ 0\,0\,0\,0\,0\,0\,1 \\ 0\,0\,0\,0\,1\,0\,0 \end{bmatrix} \tag{60}$$

PWM method is used to control the proposed converter like single-switch multiple-outputs converters in [23], [32]–[35]. The PWM control diagram is shown in Fig. 9 which is used to regulate three output voltages. The controller directly senses and regulates V_{O2}, and LUO side output voltage (V_{O1}) and boost side output voltage (V_{O3}) are indirectly regulated. In the proposed converter, coupled inductor at the output side is connected to three output ports. So, the outputs in the proposed converter are related to each other and it is enough to feedback from only one output. This is another advantage of the proposed converter with respect to some multi-output converters in [2], [21], [34].

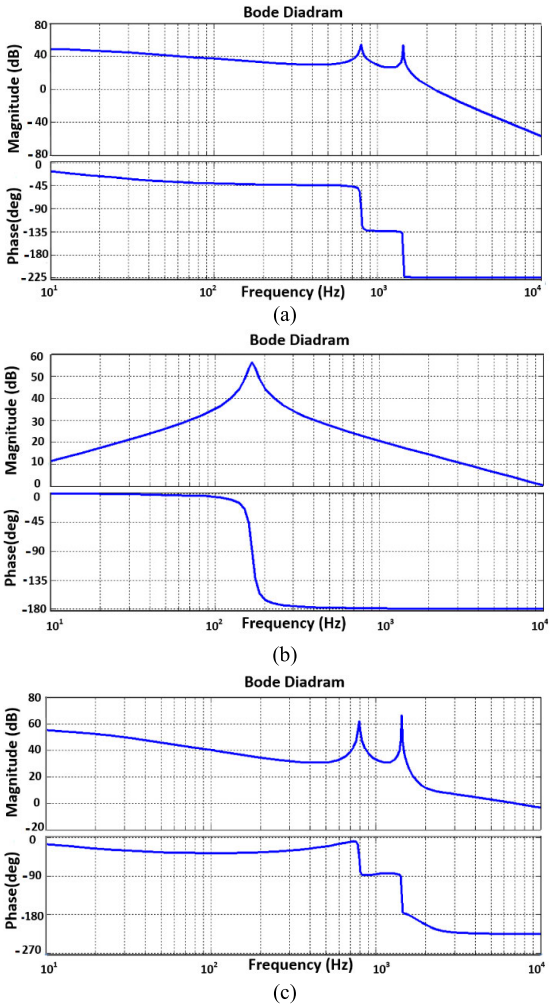

FIGURE 8. Simulated transfer function (a) control to Vo_1 (b) control to Vo_2 (c) control to Vo_3.

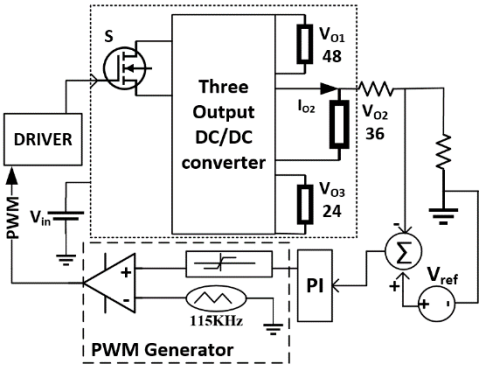

FIGURE 9. Control scheme of the proposed converter.

IV. EXPERIMENTAL RESULTS

In order to confirm the theoretical analysis, a 110W CCM prototype is implemented. Fig. 10 shows the prototype of the proposed converter. The 110W proposed converter is assumed to operate with 12V input voltage 48V, 36V, and 24V output voltages with 115 kHz switching frequency. The loads are $R_{O1} = 30\Omega$, $R_{O2} = 100\Omega$ and $R_{O3} = 30\Omega$. By considering the output voltages $V_{O1} = 48$V and based on (14), the duty cycle (d) can be obtained equal to 0.66. Considering the duty cycle and known output voltages, $V_{O2} = 36$V and

TABLE 4. Comparison between the proposed converter and similar converters.

Ref.	`Di: Diode S:Switch C:Capacitor L:inductor G: Voltage Gain d: Duty Cycle												
	Di	S	C	L	Core	Total No.	Outputs No.	G1	G2	G3	$V_{S,Max}$(Actual)	Switch Spike	Efficiency%
[2]	4	3	7	1	1	16	2	$\frac{2(N+1)}{d_1}$	$\frac{1-d_3}{d_1}$	-	$\frac{V_{in}}{d}>$	Yes	92
[21]	1	2	2	2	0	7	2	$\frac{1}{1-d}$	d_2	-	V_{out}	No	90
[36]	1	2	3	3	0	9	2	$\frac{d_1}{1-d_1}$	$\frac{d_1+d_2-1}{1-d_1}$	-	$V_{in}+V_{out}$	No	91
[14]	5	1	6	2	1	15	3	$\frac{1}{1-d_1-d_x}$	$\frac{N+1}{1-d}$	≈ 1.1	$\frac{V_{out2}}{1+N}>$	Yes	94
[16]	4	1	5	1	1	12	3	$\frac{N+d}{1-d}$	$\frac{1}{1-d_1-d_x}$	$\frac{1}{1-d}$	$\frac{V_{in}}{1-d}>$	Yes	94
[19]	7	2	7	2	0	18	3	$\frac{2}{1-d}$	$\frac{1}{1-d}$	$\frac{3+d}{1-d}$	$\frac{V_{in}}{1-d}$	No	92
[23]	3	1	5	3	0	12	3	$\frac{d}{1-d}$	$\frac{d}{1-d}$	$\frac{1}{1-d}$	$\frac{V_{in}}{1-d}$	No	82
Proposed	4	1	4	0	1	10	3	$\frac{2-d}{1-d}$	$\frac{dN_B}{1-d}$	$\frac{1+d/N_A}{1-d}$	$\frac{V_{in}}{1-d}$	No	92.5

V_{O3} = 24V, turn ratios of N_B and N_A is determined based on (15), and (16) respectively. According to (21), minimum amount of magnetizing inductance (L_m) is obtained. To guarantee CCM operation, 197μH magnetizing inductance is implemented. By known N_A, N_B, and L_m, the value of L_2 and L_3 is calculated using (22) and (23). The converter components and specifications are showed in Table 3. In order to select right semiconductors, the corresponding voltage, and current stresses is considered using Table 1. Therefore, IRFP260, for MOSFET, and BYV32-200 for diodes, is selected. Fig. 11a shows voltage and current waveforms of the switch S. The L_1 current in Fig. 11b, D_1 current and voltage in Fig. 11c, voltage and current of C_1 in Fig. 11d, D_2, D_3, and D_4 are in Figures 11e, 11f, and 11g respectively verifying theoretical waveforms. The output voltages V_{O1} and V_{O2} are shown in Fig. 11h and the isolated output flyback part is presented in Fig. 11i.

Since the energy stored in the leakage inductance is released through the diode D_1 and C_1 in switching turn-off instant, there is no voltage spike across the switch (Fig.11a), which is an advantage of the proposed converter leading to low switch stress and capacitive turn-on losses. Meanwhile, the Luo structure of the proposed converter minimizes the output current ripple and maintains the conversion efficiency at high power levels. In addition, the super lift Luo converter section, donates high-power density, higher voltage gain, and a less complicated structure as well. A single core is employed for three-coupled inductor as another advantage of the converter. Moreover, the three outputs connected to one coupled inductor and it is sufficient to have a feedback only from one sensitive output unlike the control circuit in [34] in which feedbacks from all outputs are needed.

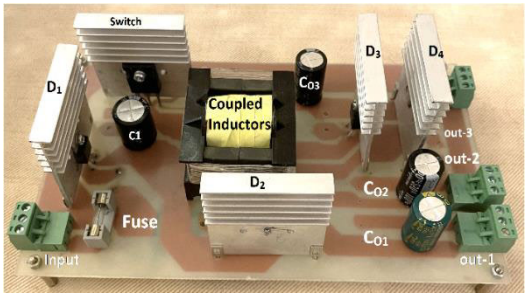

FIGURE 10. Prototype of the proposed converter.

The transient responses of the proposed converter under step output-power changes between 65W and 110 W are shown in Fig. 12. Although there are tiny voltage variations under step output power alterations, the output voltage levels is properly regulated. The output voltage responses of the proposed converter under the nominal input voltage 12V to be varied 10% are represented in Fig. 13. Even though there are slight voltage variations under input voltage change from 12V to 13.2V, three output voltages can be steadily adjusted at desired values.

Power losses of the proposed converter are displayed in Fig. 14. The most power losses percentage belongs to diodes. Fig. 15 shows the efficiency curve of the proposed converter in comparison to [23], which is a three outputs SEPIC-Cuk-Boost converter at a similar condition. The efficiency is about 92.5% at the nominal output power for the proposed converter.

Table 4 compares the features of the proposed SIMO converter with similar previous papers. The efficiency of

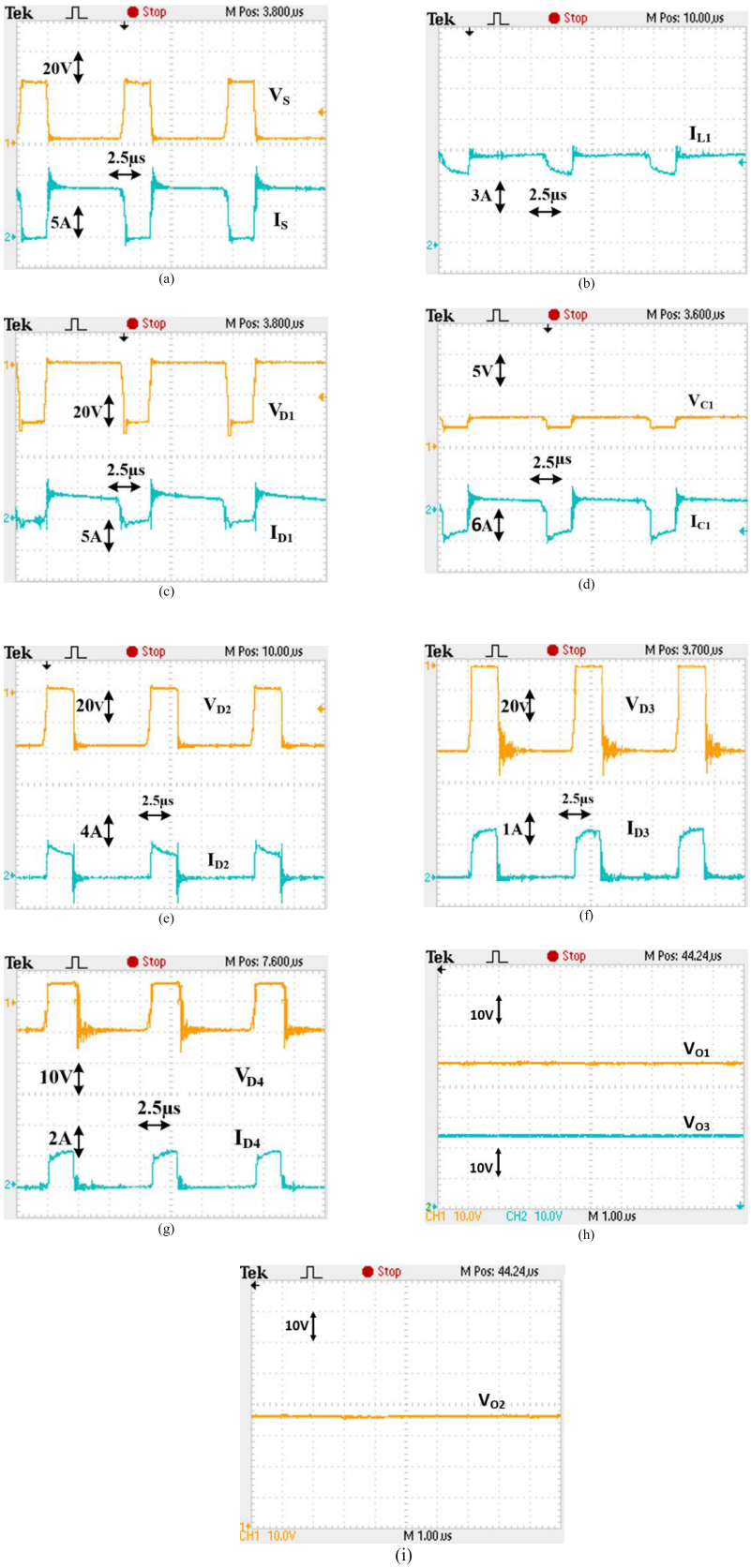

FIGURE 11. Experimental waveforms (a) Drain-source voltage and Switch current (b) I_{L1} (c) V_{D1} and I_{D1} (d) V_{C1} and I_{C1} (e) V_{D2} and I_{D2} (f) V_{D3} and I_{D3} (g) V_{D4} and I_{D4} (h) V_{O1} and V_{O3} (i) V_{O2}.

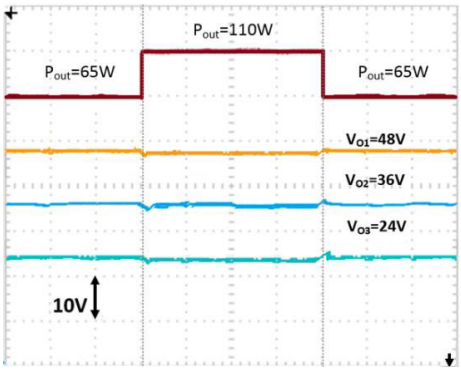

FIGURE 12. Measured transient responses of proposed converter under step output-power variation.

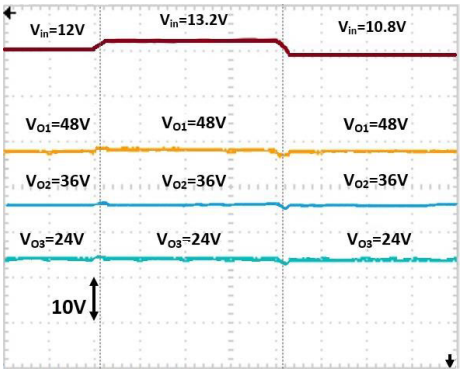

FIGURE 13. Measured transient responses of proposed converter under input voltage variations.

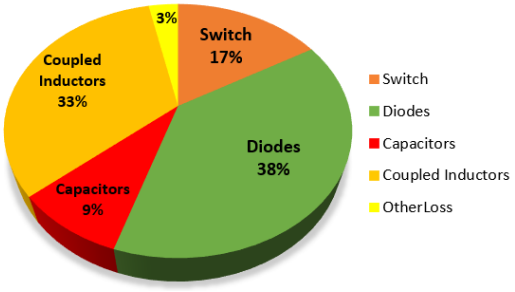

FIGURE 14. Power losses of components in the proposed converter.

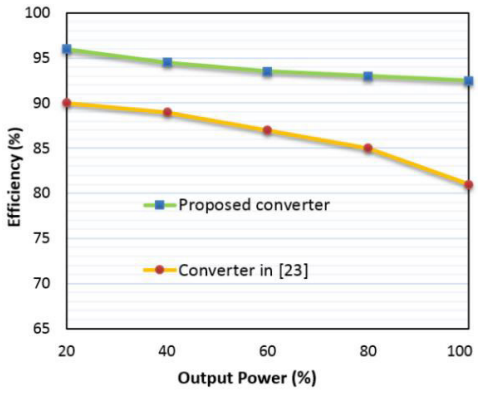

FIGURE 15. Efficiency curve of the proposed converter and [26].

converters has also shown in Table 4 at the nominal output power equal to 110W[2] requires three switches and voltage

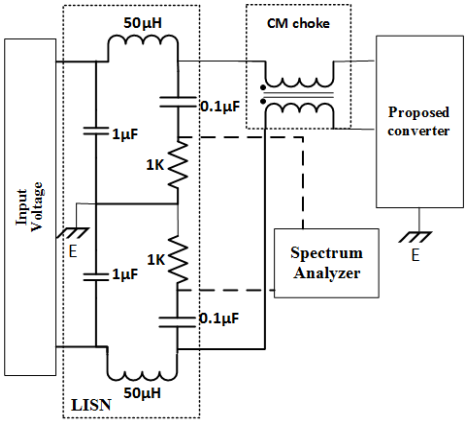

FIGURE 16. Block diagram of conducted EMI measurement with CM choke filter.

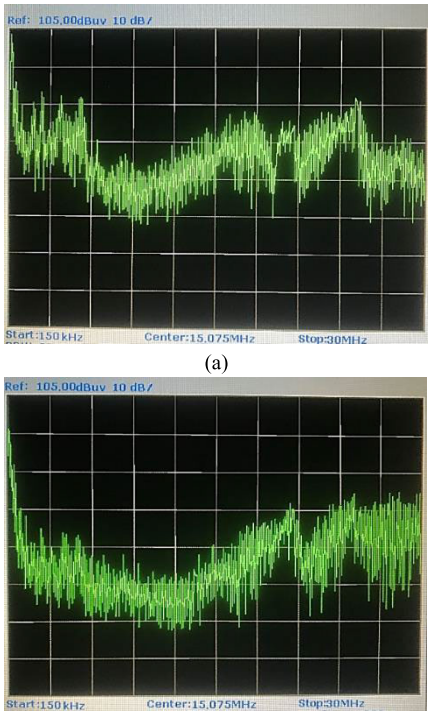

FIGURE 17. Conducted EMI measurement of the proposed converter: (a) without CM choke (b) with CM choke. Vertical axis: 25–105 dBμV; Horizontal axis: 0.15 M–30 MHz.

spike on one switch with two outputs. Although [21], [36] with two outputs possess has low number of elements, the voltage gain is low. [14] and [16] have high gain in one output and better efficiency by using soft switching technique. However, there are spike voltages and the switch has high voltage stress. A converter without spike on its two switches is introduced in [19], but a large amount of passive components is used and the voltage gain may be sensitive to parasitic parameters. Reference [23] has insignificant voltage gain in all outputs considering its component counts. Compared to other three outputs SIMO converters, the proposed converter

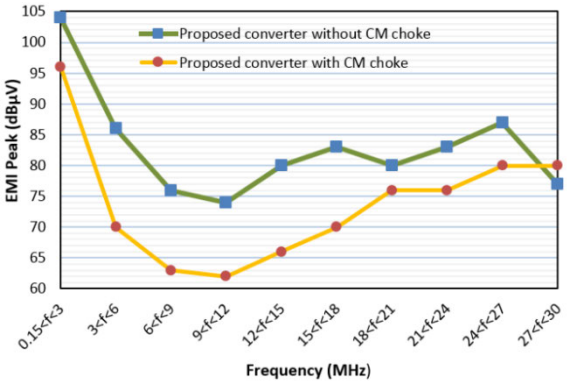

FIGURE 18. Comparison between experimental results of conducted electromagnetic emissions for the proposed converter with or without CM choke EMI filter.

has a low number of elements without voltage spike on its single switch even using coupled inductor.

V. CONDUCTED EMI MEASUREMENT

Conducted EMI of the proposed converter without and with 1mH common-mode (CM) choke are measured using CISPR 22 line impedance stabilization network (LISN) as shown in Fig. 16. In Figures 17 (a) and 17(b), the main conducted EMI peak is compared which verified the benefit of applying CM choke as a cost-effective and simple solution for the proposed converter. In most frequencies, the EMI main peak is significantly reduced. The reduction value reaches around 15dB at 3-18 MHz frequency band as is clear in Fig. 18.

VI. CONCLUSION

In this paper, a single switch step-up DC-DC converter with three outputs based on Luo topology is proposed. The operation analysis, design considerations, dynamic response, and losses are discussed. The 110W prototype verifies the theoretical analysis such as low switch voltage stress and low output current ripple with three step-up outputs with one switch and magnetic core. By recycling leakage inductance energy, there is no voltage spike across the switch, which is the main advantage of converters with coupled inductor. The proposed converter provides efficiency around 92.5% at full load. The conducted electromagnetic interference (EMI) is also evaluated and reduced by a CM choke as a simple and cost-effective method.

REFERENCES

[1] M. Forouzesh, K. Yari, A. Baghramian, and S. Hasanpour, "Single-switch high step-up converter based on coupled inductor and switched capacitor techniques with quasi-resonant operation," *IET Power Electron.*, vol. 10, no. 2, pp. 240–250, Feb. 2017.

[2] S. Song, G. Chen, Y. Liu, Y. Hu, K. Ni, and Y. Wang, "A three-switch-based single-input dual-output converter with simultaneous boost & buck voltage conversion," *IEEE Trans. Ind. Informat.*, vol. 16, no. 7, pp. 4468–4477, Jul. 2020.

[3] S.-W. Seo, J.-H. Ryu, Y. Kim, and J.-B. Lee, "Ultra-high step-up interleaved converter with low voltage stress," *IEEE Access*, vol. 9, pp. 37167–37178, 2021.

[4] D. Yu, J. Yang, R. Xu, Z. Xia, H.-H. C. Iu, and T. Fernando, "A family of module-integrated high step-up converters with dual coupled inductors," *IEEE Access*, vol. 6, pp. 16256–16266, 2018.

[5] C. Wang, M. Li, Z. Ouyang, and G. Wang, "Resonant push–pull converter with flyback regulator for MHz high step-up power conversion," *IEEE Trans. Ind. Electron.*, vol. 68, no. 2, pp. 1178–1187, Feb. 2021.

[6] N. Mohammadian and M. R. Yazdani, "Half-bridge flyback converter with lossless passive snubber and interleaved technique," *IET Power Electron.*, vol. 11, no. 2, pp. 239–245, Feb. 2018.

[7] K. Tseng, H. Huang, and C. Cheng, "Integrated boost-forward-flyback converter with high step-up for green energy power-conversion applications," *IET Power Electron.*, vol. 14, no. 1, pp. 27–37, Jan. 2021.

[8] M. E. Azizkandi, F. Sedaghati, H. Shayeghi, and F. Blaabjerg, "A high voltage gain DC–DC converter based on three winding coupled inductor and voltage multiplier cell," *IEEE Trans. Power Electron.*, vol. 35, no. 5, pp. 4558–4567, May 2020.

[9] M. Mahmoudi, A. Ajami, and E. Babaei, "A non-isolated high step-up DC–DC converter with integrated 3 winding coupled inductor and reduced switch voltage stress," *Int. J. Circuit Theory Appl.*, vol. 46, no. 10, pp. 1879–1898, Oct. 2018.

[10] H. Radmanesh, M. R. Soltanpour, and M. E. Azizkandi, "Design and implementation of an ultra-high voltage DC–DC converter based on coupled inductor with continuous input current for clean energy applications," *Int. J. Circuit Theory Appl.*, vol. 49, no. 2, pp. 348–379, Feb. 2021.

[11] T. Nouri, N. Nouri, and N. Vosoughi, "A novel high step-up high efficiency interleaved DC–DC converter with coupled inductor and built-in transformer for renewable energy systems," *IEEE Trans. Ind. Electron.*, vol. 67, no. 8, pp. 6505–6516, Aug. 2020.

[12] T. Meng, H. Ben, and C. Li, "An input-series flyback converter with the coupled-inductor-based passive snubber for high-input voltage multiple-output applications," *IEEE Trans. Ind. Electron.*, vol. 66, no. 6, pp. 4344–4355, Jun. 2019.

[13] K.-C. Tseng, J.-Z. Chen, J.-T. Lin, C.-C. Huang, and T.-H. Yen, "High step-up interleaved forward-flyback boost converter with three-winding coupled inductors," *IEEE Trans. Power Electron.*, vol. 30, no. 9, pp. 4696–4703, Sep. 2015.

[14] R.-J. Wai and K.-H. Jheng, "High-efficiency single-input multiple-output DC–DC converter," *IEEE Trans. Power Electron.*, vol. 28, no. 2, pp. 886–898, Feb. 2013.

[15] S. K. Mishra, K. K. Nayak, M. S. Rana, and V. Dharmarajan, "Switched-boost action based multiport converter," *IEEE Trans. Ind. Appl.*, vol. 55, no. 1, pp. 964–975, Jan. 2019.

[16] R.-J. Wai and Z.-F. Zhang, "High-efficiency single-input triple-outputs DC–DC converter with zero-current switching," *IEEE Access*, vol. 7, pp. 84952–84966, 2019.

[17] M. Z. Malik, H. M. H. Farh, A. M. Al-Shaalan, A. A. Al-Shamma'a, and H. H. Alhelou, "A novel single-input-multi-output converter for flexible-order power-distributive with MPPT capability," *IEEE Access*, vol. 9, pp. 131020–131032, 2021.

[18] P. Mohseni, S. H. Hosseini, M. Sabahi, T. Jalilzadeh, and M. Maalandish, "A new high step-up multi-input multi-output DC–DC converter," *IEEE Trans. Ind. Electron.*, vol. 66, no. 7, pp. 5197–5208, Jul. 2019.

[19] Z. Saadatizadeh, P. C. Heris, E. Babaei, and M. Sabahi, "A new nonisolated single-input three-output high voltage gain converter with low voltage stresses on switches and diodes," *IEEE Trans. Ind. Electron.*, vol. 66, no. 6, pp. 4308–4318, Jun. 2019.

[20] B. Faridpak, M. Farrokhifar, M. Nasiri, A. Alahyari, and N. Sadoogi, "Developing a super-lift Luo-converter with integration of buck converters for electric vehicle applications," *CSEE J. Power Energy Syst.*, vol. 7, no. 4, pp. 811–820, 2021.

[21] O. Ray, A. P. Josyula, S. Mishra, and A. Joshi, "Integrated dual-output converter," *IEEE Trans. Ind. Electron.*, vol. 62, no. 1, pp. 371–382, Jan. 2015.

[22] O. Mourra, A. Fernandez, F. Tonicello, and S. Landstroem, "Multiple port DC DC converter for spacecraft power conditioning unit," in *Proc. 27th Annu. IEEE Appl. Power Electron. Conf. Expo. (APEC)*, Feb. 2012, pp. 1278–1285.

[23] M. B. F. Prieto, S. P. Litran, E. D. Aranda, and J. M. E. Gomez, "New single-input, multiple-output converter topologies: Combining single-switch nonisolated DC–DC converters for single-input, multiple-output applications," *IEEE Ind. Electron. Mag.*, vol. 10, no. 2, pp. 6–20, Jun. 2016.

[24] S. Song, K. Ni, G. Chen, Y. Hu, and D. Yu, "Multi-output LED driver integrated with 3-switch converter and passive current balance for portable applications," *J. Power Electron.*, vol. 19, no. 1, pp. 58–67, Jan. 2019.
[25] F. L. Luo and H. Ye, *Essential DC/DC Converters*. Boca Raton, FL, USA: CRC Press, 2018.
[26] F. L. Luo and H. Ye, "Positive output super-lift converters," *IEEE Trans. Power Electron.*, vol. 18, no. 1, pp. 105–113, Jan. 2003.
[27] F. L. Luo, H. Ye, and H. Ye, *Advanced DC/DC Converters*, 2nd ed. Boca Raton, FL, USA: CRC Press, 2016.
[28] L.-S. Yang, "Implementation of high step-up DC–DC converter using voltage-lift and coupled inductor techniques," *Int. J. Circuit Theory Appl.*, vol. 46, no. 11, pp. 2079–2097, Nov. 2018.
[29] B. Singh and R. Kushwaha, "Power factor preregulation in interleaved Luo converter-fed electric vehicle battery charger," *IEEE Trans. Ind. Appl.*, vol. 57, no. 3, pp. 2870–2882, May 2021.
[30] G. Jothimani, Y. Palanichamy, S. K. Natarajan, and T. Rameshkumar, "Single-phase front-end modified interleaved Luo power factor correction converter for on-board electric vehicle charger," *Int. J. Circuit Theory Appl.*, vol. 49, no. 9, pp. 2655–2669, Sep. 2021.
[31] F. L. Luo and H. Ye, "Hybrid split capacitors and split inductors applied in positive output super-lift Luo-converters," *IET Power Electron.*, vol. 6, no. 9, pp. 1759–1768, 2013.
[32] S. Patil, R. S. Geetha, B. L. Santosh, B. K. Singh, and V. Chippalkatti, "Design and implementation of multiple output forward converter with Mag-amp and LDO as post regulators for space application," *Int. J. Eng., Sci. Technol.*, vol. 12, no. 3, pp. 43–56, Sep. 2020.
[33] M. Tahan, D. O. Bamgboje, and T. Hu, "Compensated single input multiple output flyback converter," *Energies*, vol. 14, no. 11, p. 3009, May 2021.
[34] B. M. Rao, K. Nagalingachari, and L. S. Ram, "Closed loop control of single-input multiple-output DC–DC converter," *Int. Res. J. Eng. Technol.*, vol. 2, no. 3, pp. 782–788, 2015.
[35] I. A. Aden, H. Kahveci, and M. E. Sahin, "Single input, multiple output DC–DC buck converter for electric vehicles," *Turkish J. Electromech. Energy*, vol. 2, no. 2, pp. 7–13, Jan. 2017.
[36] G. Chen, Z. Jin, Y. Deng, X. He, and X. Qing, "Principle and topology synthesis of integrated single-input dual-output and dual-input single-output DC–DC converters," *IEEE Trans. Ind. Electron.*, vol. 65, no. 5, pp. 3815–3825, May 2018.

FERESHTEH GHASEMI was born in Esfahan, Iran, in 1979. She received the B.S. and M.S. degrees in electrical engineering from Islamic Azad University, Najafabad Branch, Iran, in 2001 and 2004, respectively. She is currently pursuing the Ph.D. degree with Islamic Azad University, Isfahan (Khorasgan) Branch, Isfahan, Iran. Her research interests include power electronics and DC-DC converters.

MOHAMMAD ROUHOLLAH YAZDANI (Member, IEEE) was born in Isfahan, Iran, in 1978. He received the B.S. degree in electrical engineering from the Isfahan University of Technology, Najafabad Branch, in 2001, the M.S. degree in electrical engineering from Islamic Azad University, Science and Research Branch, in 2004, and the Ph.D. degree in electrical engineering from Islamic Azad University, in 2011. Since 2011, he has been an Associate Professor at the Faculty of Engineering, Islamic Azad University, Isfahan (Khorasgan) Branch, Isfahan. His research interests include switching power converters and EMI and EMC issues.

MAJID DELSHAD was born in Isfahan, Iran, in 1979. He received the B.S. degree in electrical engineering from Kashan University, Iran, in 2001, and the M.S. and Ph.D. degrees in electrical engineering from the Isfahan University of Technology, Iran, in 2004 and 2010, respectively. He is currently an Associate Professor at the Faculty of Engineering, IAU, Isfahan (Khorasgan) Branch. His research interests include soft switching in DC-DC converters and current-fed converters.